communications
chemistry

ARTICLE

https://doi.org/10.1038/s42004-021-00488-0

OPEN

Asymmetric azide-alkyne Huisgen cycloaddition on chiral metal surfaces

Samuel Stolz [1,2], Michael Bauer [3], Carlo A. Pignedoli[1], Nils Krane[1], Max Bommert[1], Elia Turco[1], Nicolò Bassi[1], Amogh Kinikar[1], Néstor Merino-Dìez [1], Roland Hany[3], Harald Brune [2], Oliver Gröning[1] & Roland Widmer [1]✉

Achieving fundamental understanding of enantioselective heterogeneous synthesis is marred by the permanent presence of multitudinous arrangements of catalytically active sites in real catalysts. In this study, we address this issue by using structurally comparatively simple, well-defined, and chiral intermetallic PdGa{111} surfaces as catalytic substrates. We demonstrate the impact of chirality transfer and ensemble effect for the thermally activated azide-alkyne Huisgen cycloaddition between 3-(4-azidophenyl)propionic acid and 9-ethynylphenanthrene on these threefold symmetric intermetallic surfaces under ultrahigh vacuum conditions. Specifically, we encounter a dominating ensemble effect for this reaction as on the Pd_3-terminated PdGa{111} surfaces no stable heterocoupled structures are created, while on the Pd_1-terminated PdGa{111} surfaces, the cycloaddition proceeds regioselectively. Moreover, we observe chirality transfer from the substrate to the reaction products, as they are formed enantioselectively on the Pd_1-terminated PdGa{111} surfaces. Our results evidence a determinant ensemble effect and the immense potential of PdGa as asymmetric heterogeneous catalyst.

---

[1] Empa, Swiss Federal Laboratories for Materials Science and Technology, Nanotech@Surfaces Laboratory, Dübendorf, Switzerland. [2] Institute of Physics, École Polytechnique Fédérale de Lausanne, Lausanne, Switzerland. [3] Empa, Swiss Federal Laboratories for Materials Science and Technology, Laboratory for Functional Polymers, Dübendorf, Switzerland. ✉email: roland.widmer@empa.ch

In recent years, on-surface synthesis under ultrahigh vacuum (UHV) conditions has emerged as a very successful method to produce extended, covalently bonded macro-molecules, which are inaccessible to wet-chemical synthesis due to insolubility or high reactivity[1]. On-surface synthesis is based on the controlled reaction of dedicated precursor molecules on well-defined single-crystal surfaces mostly by thermal activation. Although in recent years, the catalog of on-surface reactions and synthesized structures broadened extensively, the focus rarely lay on enantioselective synthesis, which is of immense importance for instance in pharmaceutical, agricultural, or food industry[2,3]. This lack of enantioselective on-surface synthesis originates largely from the scarcity of intrinsically chiral, catalytically active, and well-characterized single-crystal surfaces needed for this task. One option to circumvent this deficiency is to render achiral surfaces chiral via the adsorption of enantiopure molecules[4–10]. This approach has proven very successful under ambient conditions, for instance, in the asymmetric hydrogenation of activated ketones and asymmetric hydrogenation of prochiral olefins[11].

Intrinsically chiral metal surfaces promise an increased thermal stability, a reduction of complexity arising from the multitude of molecule–molecule arrangements and interactions, and would not require enantiopure molecular modifiers, but are accompanied by a reduced adjustability towards specific reactions. In this context, high Miller-index surfaces of achiral crystals[12,13], which exhibit a low density of chiral centers only at the kink sites of atomic steps separating adjacent terraces of low-index surfaces, have been established for enantioselective decomposition reactions under UHV conditions[14,15].

Low Miller-index surfaces of intrinsically chiral bulk crystals possess a high density of well-defined and thermally stable chiral centers. Even though chiral metallic crystals gain increasing attention in the context of topological electronic properties[16–23], in-depth characterization of their surface structure is very limited. Currently, the only intrinsically chiral and catalytically active single crystal whose low-index surfaces are well-characterized is intermetallic PdGa. PdGa belongs to the non-centrosymmetric space-group $P2_13$ (ref. [24]), and thus exists in two enantiomorphs, denoted as PdGa:A and PdGa:B[25]. Here, we focus on the two structurally dissimilar, bulk-truncated, threefold symmetric PdGa:A($\bar{1}\bar{1}\bar{1}$) and PdGa:A(111) surfaces, of which the former is terminated by isolated Pd trimers, further referred to as A:Pd$_3$ (Fig. 1a), while the top layer of the latter consists of single, isolated Pd atoms, and is denoted A:Pd$_1$ (Fig. 1b)[26]. Owing to their differing surface terminations, in combination with their equal lattice parameters, identical symmetry, and similar electronic properties, the PdGa{111} surfaces are ideally suited to disentangle ensemble and ligand effects, i.e., the influence of the local geometric and electronic properties, respectively, in asymmetric heterogeneous catalysis[27–30].

Chirality transfer from the PdGa{111} surfaces onto molecular processes has been demonstrated with acetylene (C_2H_2; achiral) and 9-ethynylphenanthrene (9-EP; prochiral, thus appearing in two distinguishable surface enantiomers R and S when confined to a planar configuration)[31,32]. Specifically, C_2H_2 has been reported to exhibit directed rotation on the Pd$_3$-terminated PdGa{111} surfaces[31]. On the other hand, for 9-EP, enantiopure trimerization from an initial racemic mixture of monomers on the Pd$_3$- and enantioselective adsorption of individual monomers on the Pd$_1$-terminated PdGa{111} surfaces have been shown[32].

Therefore, 9-EP promotes itself as prototypical alkyne precursor for investigating enantioselective synthesis on the PdGa{111} surfaces. Moreover, on-surface azide–alkyne Huisgen cycloaddition (Fig. 1c) without emphasis on enantioselectivity has been successfully demonstrated on Au(111)[33], and, using 9-EP as precursor, on Cu(111) under UHV conditions by Bebensee et al.[34]. This catalytically activated reaction, which belongs to the class of Click Chemistry, selectively yields 1,4-triazole regioisomers and omits the formation of 1,5-triazoles. According to the d-band model introduced by Liu and Nørskov[28] and Nørskov et al.[35], PdGa is expected to possess similar catalytic activity for the azide–alkyne Huisgen cycloaddition as copper. To perform the reaction, we chose commercially available prochiral 3-(4-azidophenyl)propionic acid (APA) as azide reactant (Fig. 1d).

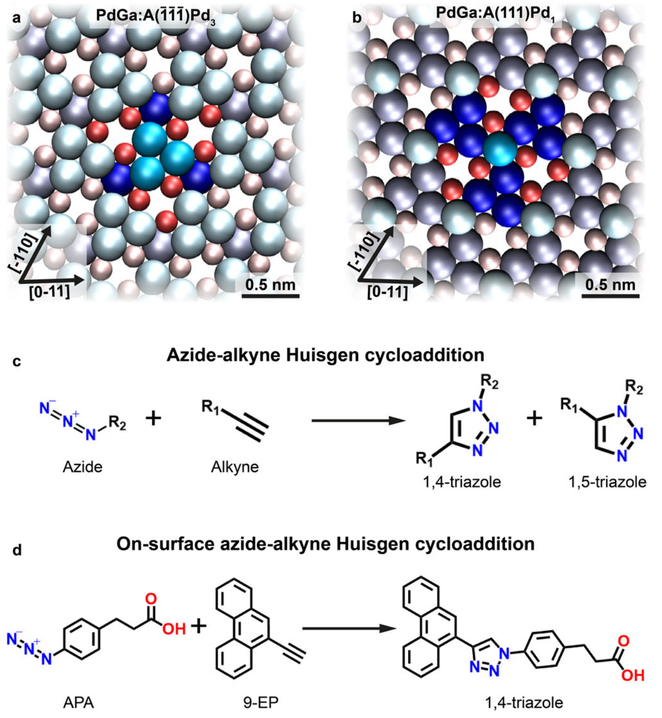

Fig. 1 Schematics of the PdGa{111} surfaces and the azide–alkyne Huisgen cycloaddition. The atomic surface structure of **a** PdGa:A($\bar{1}\bar{1}\bar{1}$)Pd$_3$ (first layer Pd$_3$ in bright blue: $z = 0$ pm; second layer Ga$_3$ in red: $z = -85$ pm; third layer Pd$_1$ in dark blue: $z = -161$ pm) and **b** PdGa:A(111)Pd$_1$ (first layer Pd$_1$ in bright blue: $z = 0$ pm; second layer Ga$_3$ in red: -57.4 pm; third layer Pd$_3$ in dark blue: -149.8 pm) with their chirality highlighted by a top layer Pd trimer or a single top layer atom, respectively, and their neighbors in saturated colors. **c** General reaction scheme of the azide–alkyne Huisgen cycloaddition. **d** The investigated on-surface Huisgen cycloaddition between 9-ethynylphenanthrene (9-EP) and 3-(4-azidophenyl)propionic acid (APA) yielding 1,4-triazole regioisomers.

Using scanning tunneling microscopy (STM), complemented with X-ray photoelectron spectroscopy (XPS), and density functional theory (DFT) calculations, we demonstrate a significant ensemble effect on the PdGa{111} surface reactivity, manifested in the occurrence of the regio- and, most importantly, enantioselective cycloaddition between APA and 9-EP on the Pd$_1$-terminated PdGa{111} surfaces, but its suppression on Pd$_3$-terminated PdGa{111}.

Results and discussion

Azide–alkyne Huisgen cycloaddition on Pd$_3$-terminated PdGa{111} surfaces. A series of STM images of the individual deposition of 9-EP and APA molecules and the co-deposition of both molecules on A:Pd$_3$ at room temperature (RT) and after subsequent annealing to 425 and 515 K is shown in Fig. 2. As previously reported[32], 9-EP deposited at RT results in a homogeneous racemate of well isolated monomers (Fig. 2a) and formation of 9-EP trimers with increasing enantiomeric excess (ee) up to 97 ± 2% towards RRR enantiomorphs for increasing

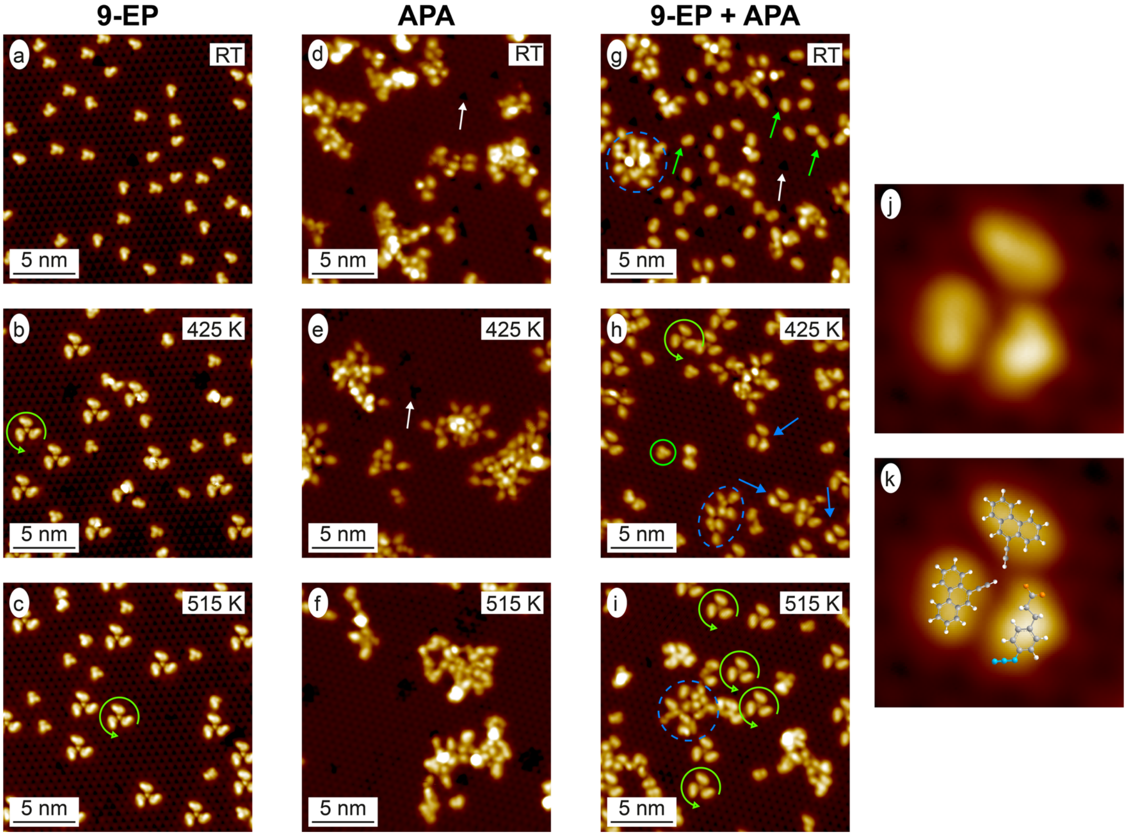

Fig. 2 Suppressed azide-alkyne Huisgen cycloaddition on the Pd$_3$-terminated PdGa{111} surfaces. STM images ($V_B = 20$ mV; $I_T = 1$ nA) of 9-EP **a** deposited on PdGa:A($\overline{1}\overline{1}\overline{1}$)Pd$_3$ at RT, and after subsequent annealing to **b** 425 K and **c** 515 K. STM images ($V_B = 200$ mV; $I_T = 0.1$ nA) of APA molecules on the PdGa:A($\overline{1}\overline{1}\overline{1}$)Pd$_3$ surface after **d** RT deposition, subsequent annealing to **e** 425 K and **f** 515 K. STM images ($V_B = 200$ mV; $I_T = 0.1$ nA) of APA co-adsorbed with 9-EP after **g** RT deposition, subsequent annealing to **h** 425 K and **i** 515 K. High-resolution STM image (3 × 3 nm^2; $V_B = 20$ mV; $I_T = 0.2$ nA) of the frequently observed molecular structure containing one APA and two 9-EP molecules, which is marked with blue arrows in **h**, is shown in **j** and overlaid with the molecular structure in **k**. The green circular arrows in **b**, **c**, **h**, **i** highlight the homochiral 9-EP propeller, the white arrows in **d**, **e**, **g** the depression caused by APA remnants, and the green arrows in **g** a 9-EP molecule interacting with an APA remnant. The blue dashed circles in **g**, **h**, **i** indicate APA agglomerations and the green circle in **h** a 9-EP monomer.

temperatures (Fig. 2b, c). On the other hand, APA molecules deposited on A:Pd$_3$ at RT create large, disordered agglomerates (Fig. 2d). Additionally, depressions, which are absent on the pristine surface, are observed on the substrate, as indicated by the white arrow. We attribute these depressions to fragments of the decomposed carboxylic acid group of the APA molecule as they are also observed upon deposition of ex situ synthesized 1,4-triazoles (Fig. S1) and XPS investigations show a strong C 1*s* component arising from the carboxylic acid group (Fig. S2a, Table S1 and Supplementary Note 1). On the other hand, the ratio between the C 1*s* and N 1*s* XPS intensity is around three times larger than the one expected for pristine APA (Fig. S3 and Table S4). Hence also most azide groups decompose, and desorb from the surface. Subsequent annealing of the sample up to 515 K leads to a reduction of the depressions, as they desorb, while agglomeration proceeds without ever forming discernible regular structures, i.e., reoccurring structures of similar topographic signature in STM images (Fig. 2d–f).

When APA is co-deposited with 9-EP on A:Pd$_3$, no intermolecular reactions are observed at RT. While APA again agglomerates, 9-EP seems to mostly bond to the previously mentioned molecular fragments detached from APA molecules (depressions), as pointed out by the green arrow in Fig. 2g. Upon annealing to 425 K (Fig. 2h), 9-EP appears in its pristine adsorption configuration, which means it is detached from the molecular fragments, and, importantly, new prochiral 9-EP/APA heterostructures that consist of two 9-EP and one APA molecule are formed (Fig. 2j–k). The adsorption configuration of 9-EP molecules incorporated in these trimer heterostructures with respect to the PdGa substrate is identical with that of R enantiomers incorporated into pure 9-EP trimers[32]. The heterostructure trimers exclusively appear in the enantiomeric form shown in Fig. 2j, k on the A:Pd$_3$ termination. The incorporated APA is not covalently bound in these heterostructure trimers, as, upon further annealing to 515 K, these structures deplete and homostructural 9-EP trimers become the only regular motive (highlighted by a green circular arrow in Fig. 2i). Therefore, even though PdGa is copper-like with regard to the catalytic reactivity according to the d-band model[35], the azide–alkyne Huisgen cycloaddition cannot be triggered with any significant yield on the A:Pd$_3$ surface.

Azide–alkyne Huisgen cycloaddition on Pd$_1$-terminated PdGa{111} surfaces. On the A:Pd$_1$ surface, 9-EP deposited at RT adsorbs with an ee of 98% in favor of the R enantiomer (cf. Fig. 3a), and dimerizes without ee above 400 K, as reported by Prinz et al.[36]. The adsorption behavior of APA on the Pd$_1$-terminated PdGa{111} surfaces is in stark contrast to that on A:Pd$_3$, as the APA molecules barely agglomerate even at temperatures up to 415 K (Fig. 3b and Fig. S5). The most frequently observed APA structures are shown in the STM images in Fig. 3c–f.

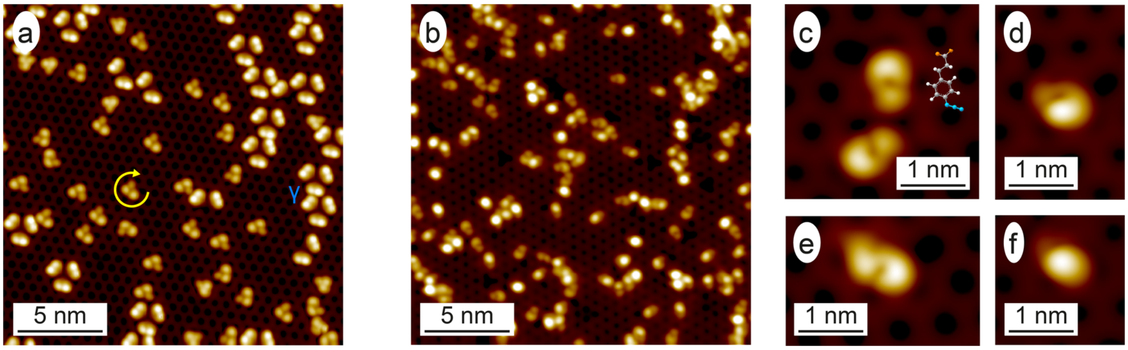

Fig. 3 Alkyne and azide on the Pd$_1$-terminated PdGa{111} surfaces. Large-scale STM images of **a** 9-EP ($V_B = 20$ mV; $I_T = 2$ nA) and **b** APA ($V_B = 100$ mV; $I_T = 0.4$ nA) deposited at RT on PdGa:A(111)Pd$_1$. **c**–**f** High-resolution STM images ($V_B = 20$ mV; $I_T = 0.2$ nA) of the different APA configurations on PdGa:A(111)Pd$_1$ with the molecular structure of APA in **c**.

The sickle-like molecular structures in Fig. 3c, e strongly resemble the terminal phenylpropionic acid group of the ex situ synthesized 1,4-triazoles adsorbed on PdGa:A(111)Pd$_1$ in Fig. S6. These two structures are attributed to pristine APA molecules, whereas their azide group only exhibits a very weak STM signal like on the less corrugated Ag(111)[37]. The coverage of the molecular structures in Fig. 3c, e relative to all APA derivatives on the Pd$_1$-terminated PdGa{111} surfaces amounts to around 30–35%, upon deposition and after annealing to 415 K (Fig. S5), which is in good agreement with the maximum amount of pristine APA molecules estimated from XPS investigations (Fig. S4 and Table S5). The molecular structures in Fig. 3d, f are APA molecules with decomposed azide group. On Pd$_1$-terminated PdGa{111} surfaces, part of the APA propionic acid groups are deprotonated (Fig. S2b and Table S2), but no signs of their detachment from APA molecules could be identified, neither with XPS nor STM.

After having clarified that around 30% of the APA monomers remain structurally intact up to 415 K on the Pd$_1$-terminated PdGa{111} surfaces, APA was co-deposited with 9-EP at RT (Fig. 4). As shown in Fig. 4a, both 9-EP and APA mainly appear as non-interacting monomers. The pronounced depressions on this surface represent Pd vacancies in the Pd$_1$-termination[26] and the apparent trimer is composed of individual 9-EP molecules adsorbed on such a vacancy[36]. 9-EP molecules appear with a relative abundance between 40 and 60% and exhibit an ee > 90%. Due to the lack of significant intermolecular interactions, also APA molecules occupy the same adsorption sites as in the case when they are adsorbed without 9-EP (cf. Fig. 3).

The cycloaddition between APA and 9-EP can be triggered thermally on Pd$_1$-terminated PdGa{111} by annealing the sample with co-deposited molecules at 425 K. This gives rise to the observation of several new covalently coupled molecular structures (Fig. 4b) in high abundance (Figs. S9 and S10 and Supplementary Note 2). About 5% of the new molecular structures are previously reported 9-EP dimers[36] (blue arrow in Fig. 4b), whereas 5% consist of one 9-EP molecule and the phenylpropionic acid moiety of APA, but are too small to be intact triazoles (Fig. S11). The vast majority (90%, green arrows Fig. 4b) of these molecular structures exhibit one of the six different STM appearances presented in Fig. 4c–g. Their STM signature is mainly planar in the vicinity of the coupling site, which excludes them to be 1,5-triazoles, as they would exhibit highly non-planar STM signatures according to DFT calculations done with CP2K[38] within the AiiDalab platform[39] (Fig. S12).

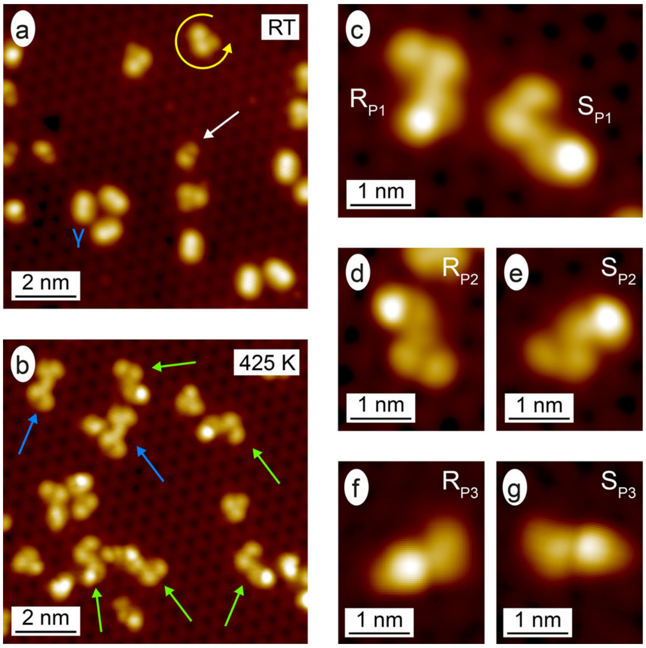

Fig. 4 Enantioselective azide–alkyne Huisgen cycloaddition on the Pd$_1$-terminated PdGa{111} surfaces. STM images ($V_B = -200$ mV; $I_T = 0.05$ nA) of **a** co-deposited APA (white arrow) and 9-EP (yellow arrow and γ-states labeled) molecules on PdGa:B($\bar{1}\bar{1}\bar{1}$)Pd$_1$, and after subsequent annealing to **b** 425 K. In **b**, the 9-EP dimers are pointed out with blue arrows, and the 1,4-triazoles with green ones. The different 1,4-triazoles are shown in detail in the high-resolution STM images ($V_B = -200$ mV; $I_T = 0.2$ nA) in **c**–**g**. **d** and **g** have been rotated to highlight the relation of the shown 1,4-triazole to the one in **e** and **f**, respectively.

To check whether the six molecular structures in Fig. 4c–g are on-surface synthesized 1,4-triazoles, we deposited ex situ synthesized 1,4-triazoles on A:Pd$_1$ held at 170 and 300 K. When imaged with STM, the ex situ synthesized 1,4-triazoles appear in three inequivalent adsorption configurations (Fig. S6). These 1,4-triazole molecules strongly resemble the reaction products formed between APA and 9-EP on the Pd$_1$-terminated PdGa{111} in terms of shape, dimensions, and adsorption geometry (Fig. S7), but differ in the intensity distribution. However, upon annealing the ex situ synthesized 1,4-triazoles to the reaction temperature of the on-surface synthesis, we observe molecular structures that are identical to those formed between APA and 9-EP on the Pd$_1$-terminated PdGa{111} surfaces (Fig. S8). This implies that the vast majority of the heterocoupled reaction products are indeed 1,4-triazoles, but with deprotonated carboxylic acid. Hence, the azide–alkyne

Table 1 Quantification of the reaction products.

Sample	1,4-Triazoles						9-EP dimer	Others
	R_{P1} 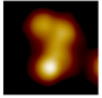	S_{P1} 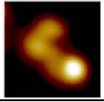	R_{P2} 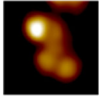	S_{P2} 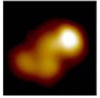	R_{P3} 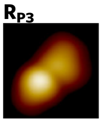	S_{P3} 		
A:Pd_1	5 ± 1%	21 ± 2%	13 ± 2%	14 ± 2%	30 ± 2%	6 ± 1%	6 ± 1%	5 ± 1%
B:Pd_1	18 ± 2%	3 ± 1%	10 ± 2%	10 ± 2%	12 ± 2%	36 ± 2%	5 ± 1%	6 ± 1%

Abundancies of the identified coupled molecular species on the PdGa:A(111)Pd_1 and PdGa:B($\bar{1}\bar{1}\bar{1}$)Pd_1 surfaces. The reaction products P1 and P3 clearly occur enantioselectively, while the products P2 appear in a racemic mixture.

Huisgen cycloaddition proceeds regioselectively on Pd_1-terminated PdGa{111} surfaces.

Asymmetric azide–alkyne Huisgen cycloaddition on Pd_1-terminated PdGa{111} surfaces. It becomes clear that the two molecules in Fig. 4c, the two in Fig. 4d, e and the ones in Fig. 4f, g are mirror images of each another, thus they represent complementary enantiomers, which will be discussed later in view of enantioselectivity. The distinctive feature in the STM signatures of the R and S enantiomers in all three cases is the arrangement of the phenylpropionic acid with respect to the phenanthrene moiety. If the phenylpropionic acid unit is perpendicular (almost parallel) to the phenanthrene moiety, the 1,4-triazoles appear L-shaped (Z-shaped) (Fig. 4c–e, the triazoles are denoted P1 and P2, respectively) or I-shaped (P3) for an intermediate orientation (Fig. 4f, g). The atomic resolution of the substrate in the STM images combined with the structure overlay allows to determine the adsorption configuration of these reaction products (Fig. S13b, e, h), whereas the enantiospecific arrangement of the propionic acid moiety remains ambiguous. The relative abundance of the three product structures P1–P3 are summarized in Table 1 for the two enantiomeric forms R and S on the Pd_1-terminated surfaces (the products are correspondingly labeled R_{P1}, S_{P1}, R_{P2},…, S_{P3}). Regarding the arrangement of the triazole with respect to the phenanthrene moiety in the 1,4-triazoles, P2 and P3 belong to the same diastereomer. Hence the reaction proceeds with a diastereomeric excess $\mathrm{de} = 100\%*\frac{P2+P3-P1}{P2+P3+P1}$ of up to 50%. Considering all 1,4-triazoles, the 9-EP moiety appear as racemic mixture, which implies that at the reaction temperature of 425 K, the chiral recognition of 9-EP by the Pd_1-terminated PdGa{111} surfaces has become insignificant. Unlike the Z-shaped products P2, which do not experience any chirality transfer, enantioselectivity is clearly expressed for the L- and I-shaped products P1 and P3, where we find ratios between the different enantiomorphs of up to 4:1 and 5:1, respectively. This enantioselective behavior is supported by deposited ex situ synthesized 1,4-triazoles pointing towards the same preferential arrangement (cf. Table S6). The opposite ratio between the different P1 and P3 enantiomers for Pd_1-terminated PdGa{111} surfaces of the A and B PdGa crystal enantiomorph strongly corroborates the conclusion of their enantioselective recognition towards the 1,4-triazoles.

Compared to investigations of the azide–alkyne Huisgen cycloaddition on Cu(111)[34], where the reaction yield is reported to be of the order of 2–10%, the formation of 1,4-triazoles on the Pd_1-terminated PdGa{111} surfaces reveals a much higher yield of up to 58%. It seems as if this yield depends mainly on the availability of intact APA molecules as the yield increases with increasing ratio between APA/9-EP (Table S7), which is expected in light of the decomposition of the azid group of APA molecules upon deposition on the Pd_1-terminated PdGa{111} surfaces.

Conclusion

In summary, we have shown that the azide–alkyne Huisgen cycloaddition between pristine 9-EP and APA occurs regio- and enantioselectively on the Pd_1-terminated PdGa{111} surfaces, i.e., forming exclusively 1,4-triazoles with an exceptionally high enantiospecifity of up to 5:1. In view of the d-band model, the Pd_1-terminated PdGa{111} surfaces behave copper-like. On the other hand, the same reaction does not proceed on the Pd_3-terminated PdGa{111} surfaces, even though these PdGa{111} surfaces exhibit very similar electronic d-band structure. We therefore conclude that the vastly dissimilar catalytic properties of the Pd_1- and Pd_3-terminated PdGa{111} surfaces for the azide–alkyne Huisgen cycloaddition primarily arise from differences in the atomic arrangement in their terminating layers, i.e., the ensemble effect.

Methods

Synthesis of 3-(4-(4-(phenanthren-9-yl)-1H-1,2,3-triazol-1-yl)phenyl)propionic acid. Chemicals and solvents were purchased from commercial sources (Merck, VWR) and were used without further purification. Reactions were carried out under argon atmosphere. Column chromatography was performed using silica gel (pore size 40–63 µm, Normasil 60® from VWR chemicals).

9-Ethynylphenanthrene (75 mg, 0.37 mmol), 3-(4-azidophenyl)propinoic acid (57 mg, 0.30 mmol), tris((1-benzyl-1*H*-1,2,3-triazol-4-yl)methyl)amine (11 mg, 0.02 mmol), copper(II) sulfate (7 mg, 0.04 mmol), and sodium ascorbate (18 mg, 0.09 mmol) were dissolved in 6 ml *N*,*N*-dimethylformamide and 2 ml water. The reaction mixture was stirred for 6 h at room temperature. Additional water was added and the product was extracted with ethyl acetate. The organic fractions were washed with water and brine and dried with anhydrous sodium sulfate. The crude product was purified by flash column chromatography with silica gel and a solvent mixture of dichloromethane/ethyl acetate/acetic acid. The triazole was precipitated from dichloromethane/*n*-heptane and isolated as a white crystalline solid (85 mg, 0.22 mmol, 72%).

Nuclear magnetic resonance. ^1H and ^{13}C NMR data were recorded at 400.2 and 100.6 MHz using a 5 mm CryoProbe™ Prodigy probe equipped with *z*-gradient on a Bruker Avance III 400 NMR spectrometer (Bruker Biospin AG, Fällanden, Switzerland). 1D ^1H and ^{13}C NMR experiments as well as 2D-correlated ^1H-^{13}C HSQC, ^1H-^{13}C HMBC, and ^1H-^1H DQF-COSY experiments were performed at 298 K using the Bruker standard pulse programs and parameter sets applying 90° pulse lengths of 11.4 µs (^1H) and 10.0 µs (^{13}C). Chemical shifts (δ in ppm) were calibrated to residual solvent peaks of $CDCl_3$ at $\delta = 7.26$ and 77.0 ppm. Coupling constants *J* are reported in Hz and ^1H NMR multiplicities are described as s = singlet, d = doublet, t = triplet, m = multiplet, and dd = doublet of doublet. High-resolution mass spectrometry was recorded on a Bruker Daltonics maXis II ESI-QTOF mass spectrometer in positive mode.

^1H NMR ($CDCl_3$, 400.2 MHz): δ 8.73 (d, $J = 8.2$ Hz, 1H), 8.45 (dd, $J = 8.2$, 1.0 Hz, 1H), 8.28 (s, 1H), 8.08 (s, 1H), 7.94 (d, $J = 7.1$ Hz, 1H), 7.82 (d, $J = 8.5$ Hz, 2H), 7.75–7.68 (m, 2H), 7.68–7.61 (m, 2H), 7.45 (d, $J = 8.5$ Hz, 2H), 3.09 (t, $J = 7.6$ Hz, 2H), 2.78 (t, $J = 7.6$ Hz, 2H).

^{13}C NMR ($CDCl_3$, 100.6 MHz): δ 174.4, 147.5, 141.2, 135.5, 131.3, 130.7, 130.6, 130.3, 130.1, 129.8, 129.0, 128.8, 128.6, 127.2, 127.0, 127.0, 126.8, 126.2, 123.1, 122.6, 120.9, 34.6, 30.2.

HR-MS (pos. ESI): *m*/*z* for [$C_{25}H_{20}N_3O_2^+$]; calculated 394.1550, found 394.1549.

Sample preparation and experiments. All experiments and sample preparations were performed under UHV conditions with a base pressure below 2×10^{-10} mbar.

The sample was prepared by repeated sputtering and annealing cycles (sputtering: 20 min, Ar^+, 1 keV; annealing: 20 min at 870 K). Both 9-ethynylphenanthrene (9-EP; 97%) and 3-(4-azidophenyl)propionic acid (APA; ≥97%) were purchased from Sigma-Aldrich and were used without further purification. 9-EP and APA were deposited by exposing the clean sample surface to the molecules held at 300 K in a pumped glass tube separated by a gate valve from the preparation chamber to prevent contamination. 9-EP and APA were pumped via individual connections with the same turbo pump to minimize the risk of cross-contamination.

3-(4-(4-(phenanthrene-9-yl)-1*H*-1,2,3-triazol-1-yl)phenyl)propionic acid, further referred to as ex situ synthesized 1,4-triazole, was deposited on the clean sample surface held at 300 K from a Knudsen cell at 490 K.

STM images were acquired with a commercial low temperature STM from Scienta Omicron operated at 5 K, if not mentioned differently, in constant-current mode.

All XPS data were recorded in normal emission configuration. XPS experiments shown in Fig. S2 were performed in-house and at room temperature using a monochromatized Al *K*α source and a Scienta R3000 display analyzer. XPS spectra shown in Figs. S3 and S4 were recorded at the X03DA beamline (PEARL endstation)[40] of the SLS synchrotron radiation facility (PSI, Villigen, Switzerland) using linearly polarized radiation with a photon energy of 760 eV and a Scienta R4000 hemispherical electron analyzer equipped with a multichannel plate detector with the sample held at 180 K.

DFT calculations. The DFT calculations were performed using the CP2K code[38] on the AiiDAlab platform[39]. The electronic states were expanded with a TZV2P Gaussian basis set[41] for C, H, N, and O species and a DZVP basis set for Pd and Ga species. A cutoff of 1200 Ry was used for the plane wave basis set. We used Norm Conserving Goedecker-Teter-Hutter pseudopotentials[42] and the PBE exchange-correlation functional[43] with the D3 dispersion corrections proposed by Grimme[44].

The Pd_1 surface was modeled by a supercell of 34.75×36.11 Å^2 corresponding to 30 surface units. To obtain the equilibrium geometries, we kept the atomic positions of the bottom seven layers of the slab fixed to the bulk positions, and all other atoms were relaxed until forces were lower than 0.005 eV/Å. To obtain simulated STM images[45] within the Tersoff-Hamann approximation[46,47] we extrapolated the electronic orbitals to the vacuum region following the approach outlined by Tersoff[47].

Data availability

The data supporting the findings of this study are included in the main text and in the Supplementary Information files, and available on archive.materialscloud.org (DOI: 10.24435/materialscloud:tx-8g).

Received: 21 July 2020; Accepted: 9 March 2021;

References

1. Clair, S. & de Oteyza, D. G. Controlling a chemical coupling reaction on a surface: tools and strategies for on-surface synthesis. *Chem. Rev.* **119**, 4717–4776 (2019).
2. Smith, S. W. Chiral toxicology: it's the same thing… only different. *Toxicol. Sci.* **110**, 4–30 (2009).
3. Kasprzyk-Hordern, B. Pharmacologically active compounds in the environment and their chirality. *Chem. Soc. Rev.* **39**, 4466–4503 (2010).
4. Stacchiola, D., Burkholder, L. & Tysoe, W. T. Enantioselective chemisorption on a chirally modified surface in ultrahigh vacuum: adsorption of propylene oxide on 2-butoxide-covered palladium(111). *J. Am. Chem. Soc.* **124**, 8984–8989 (2002).
5. Lee, I. & Zaera, F. Chiral templating of surfaces: adsorption of (S)-2-methylbutanoic acid on Pt(111) single-crystal surfaces. *J. Am. Chem. Soc.* **128**, 8890–8898 (2006).
6. Gao, F., Wang, Y., Li, Z., Furlong, O. & Tysoe, W. T. Enantioselective reactions on a Au/Pd(111) surface alloy with coadsorbed chiral 2-butanol and propylene oxide. *J. Phys. Chem. C* **112**, 3362–3372 (2008).
7. Demers-Carpentier, V. et al. Direct observation of molecular preorganization for chirality transfer on a catalyst surface. *Science* **334**, 776–780 (2011).
8. Lawton, T. J. et al. Long range chiral imprinting of Cu(110) by tartaric acid. *J. Phys. Chem. C* **117**, 22290–22297 (2013).
9. Dutta, S. & Gellman, A. J. Enantiomer surface chemistry: conglomerate versus racemate formation on surfaces. *Chem. Soc. Rev.* **46**, 7787–7839 (2017).
10. Zaera, F. Chirality in adsorption on solid surfaces. *Chem. Soc. Rev.* **46**, 7374–7398 (2017).
11. Meemken, F. & Baiker, A. Recent progress in heterogeneous asymmetric hydrogenation of C=O and C=C bonds on supported noble metal catalysts. *Chem. Rev.* **117**, 11522–11569 (2017).
12. McFadden, C. F., Cremer, P. F. & Gellman, A. J. Adsorption of chiral alcohols on 'chiral' metal surfaces. *Langmuir* **12**, 2483–2487 (1996).
13. Sholl, D. S. & Gellman, A. J. Developing chiral surfaces for enantioselective chemical processing. *AIChE J.* **55**, 2484–2490 (2009).
14. Gellman, A. J. et al. Superenantioselective chiral surface explosions. *J. Am. Chem. Soc.* **135**, 19208–19214 (2013).
15. Mhatre, B. S., Dutta, S., Reinicker, A., Karagoz, B. & Gellman, A. J. Explosive enantiospecific decomposition of aspartic acid on Cu surfaces. *Chem. Commun.* **52**, 14125–14128 (2016).
16. Sanchez, D. S. et al. Topological chiral crystals with helicoid-arc quantum states. *Nature* **567**, 500–505 (2019).
17. Rao, Z. et al. Observation of unconventional chiral fermions with long Fermi arcs in CoSi. *Nature* **567**, 496–499 (2019).
18. Lv, B. Q. et al. Observation of multiple types of topological fermions in PdBiSe. *Phys. Rev. B* **99**, 241104 (2019).
19. Schröter, N. B. M. et al. Chiral topological semimetal with multifold band crossings and long Fermi arcs. *Nat. Phys.* **15**, 759–765 (2019).
20. Yuan, Q.-Q. et al. Quasiparticle interference evidence of the topological Fermi arc states in chiral fermionic semimetal CoSi. *Sci. Adv.* **5**, eaaw9485 (2019).
21. Schröter, N. B. M. et al. Observation and control of maximal Chern numbers in a chiral topological semimetal. *Science* **369**, 179–183 (2020).
22. Yao, M. et al. Observation of giant spin-split Fermi-arc with maximal Chern number in the chiral topological semimetal PtGa. *Nat. Commun.* **11**, 2033 (2020).
23. Sessi, P. et al. Handedness-dependent quasiparticle interference in the two enantiomers of the topological chiral semimetal PdGa. *Nat. Commun.* **11**, 3507 (2020).
24. Armbrüster, M. et al. Refinement of the crystal structure of palladium gallium (1:1), PdGa. *Z. Krist. NCS* **225**, 617–618 (2010).
25. Rosenthal, D. et al. Surface investigation of intermetallic PdGa(-1-1-1). *Langmuir* **28**, 6848–6856 (2012).
26. Prinz, J. et al. Isolated Pd sites on the intermetallic PdGa(111) and PdGa(-1-1-1) model catalyst surfaces. *Angew. Chem.* **124**, 9473–9477 (2012).
27. Sachtler, W. M. H. Chemisorption complexes on alloy surfaces. *Catal. Rev. Sci. Eng.* **14**, 193–210 (1976).
28. Liu, P. & Nørskov Ligand and ensemble effects in adsorption on alloy surfaces. *Phys. Chem. Chem. Phys.* **3**, 3814–3818 (2001).
29. Prinz, J. et al. Ensemble effect evidenced by CO adsorption on the 3-fold PdGa surfaces. *J. Phys. Chem. C* **118**, 12260–12265 (2014).
30. Prinz, J. et al. Adsorption of small hydrocarbons on the three-fold PdGa surfaces: the road to selective hydrogenation. *J. Am. Chem. Soc.* **136**, 11792–11798 (2014).
31. Stolz, S., Gröning, O., Prinz, J., Brune, H. & Widmer, R. Molecular motor crossing the frontier of classical to quantum tunneling motion. *Proc. Natl. Acad. Sci. USA* **117**, 14838–14842 (2020).
32. Stolz, S. et al. Near-enantiopure trimerization of 9-ethynylphenanthrene on a chiral metal surfce. *Angew. Chem. Int. Ed.* **59**, 18179–18183 (2020).
33. Diaz Arado, O. et al. On-surface reductive coupling of aldehydes on Au(111). *Chem. Commun.* https://doi.org/10.1039/C4CC09634G (2015).
34. Bebensee, F. et al. On-surface azide–alkyne cycloaddition on Cu(111): does it "click" in ultrahigh vacuum? *J. Am. Chem. Soc.* **135**, 2136–2139 (2013).
35. Nørskov, J. K. et al. The nature of the active site in heterogeneous metal catalysis. *Chem. Soc. Rev.* **37**, 2163–2171 (2008).
36. Prinz, J., Gröning, O., Brune, H. & Widmer, R. Highly enantioselective adsorption of small prochiral molecules on a chiral intermetallic compound. *Angew. Chem. Int. Ed.* **54**, 3902–3906 (2015).
37. Hellerstedt, J. et al. Aromatic azide transformation on the Ag(111) surface studied by scanning probe microscopy. *Angew Chem. Int. Ed.* **58**, 2266–2271 (2019).
38. Hutter, J., Iannuzzi, M., Schiffmann, F. & Vandevondele, J. Cp2k: atomistic simulations of condensed matter systems. *Wiley Interdiscip. Rev. Comput. Mol. Sci.* **4**, 15–25 (2014).
39. Pizzi, G., Cepellotti, A., Sabatini, R., Marzari, N. & Kozinsky, B. AiiDA: automated interactive infrastructure and database for computational science. *Comput. Mater. Sci.* **111**, 218–230 (2016).
40. Muntwiler, M. et al. Surface science at the PEARL beamline of the Swiss light source. *J. Synchrotron Radiat.* **24**, 354–366 (2017).
41. VandeVondele, J. & Hutter, J. Gaussian basis sets for accurate calculations on molecular systems in gas and condensed phases. *J. Chem. Phys.* **127**, 114105 (2007).
42. Goedecker, S., Teter, M. & Hutter, J. Separable dual-space Gaussian pseudopotentials. *Phys. Rev. B* **54**, 1703–1710 (1996).
43. Perdew, J. P., Burke, K. & Ernzerhof, M. Generalized gradient approximation made simple. *Phys. Rev. Lett.* **77**, 3865–3868 (1996).
44. Grimme, S., Antony, J., Ehrlich, S. & Krieg, H. A consistent and accurate ab initio parametrization of density functional dispersion correction (DFT-D) for the 94 elements H-Pu. *J. Chem. Phys.* **132**, 154104 (2010).
45. Talirz, L. https://github.com/ltalirz/asetk (2015).

46. Tersoff, J. D. & Hamann, D. R. in *Scanning Tunneling Microscopy* (ed. Neddermeyer, H.) 59–67 (Springer Netherlands, 1985).
47. Tersoff, J. D. Method for the calculation of scanning tunneling microscope images and spectra. *Phys. Rev. B* **40**, 11990–11993 (1989).

Acknowledgements

This work was supported by the Swiss National Science Foundation under Grant No. 159690. Calculations were supported by a grant from the Swiss National Supercomputing Centre (CSCS). For the XPS experiments at the X03DA (PEARL) beamline at the Swiss Light Source, Paul Scherrer Institut, Villigen, Switzerland, we thank the beamline scientist Matthias Muntwiler for his support during the experiments.

Author contributions

R.W. conceived and initiated the project in collaboration with H.B. and O.G.; S.S. performed the measurements with assistance of N.K.; M. Bommert, E.T., N.B., A.K., N.M.-D., and R.W. performed the D.F.T. calculations under the supervision of C.A.P. and analyzed the data under supervision of R.W.; M. Bauer synthesized the ex situ 1,4-triazoles under the supervision of R.H.; and S.S. wrote the manuscript with input from all co-authors.

Competing interests

The authors declare no competing interests.

Additional information

Supplementary information The online version contains supplementary material available at https://doi.org/10.1038/s42004-021-00488-0.

Correspondence and requests for materials should be addressed to R.W.

Reprints and permission information is available at http://www.nature.com/reprints

Supporting information for

Asymmetric azide-alkyne Huisgen cycloaddition on chiral metal surfaces

Samuel Stolz[1,2], Michael Bauer[3], Carlo A. Pignedoli[1], Nils Krane[1], Max Bommert[1], Elia Turco[1], Nicolo Bassi[1], Amogh Kinikar[1], Néstor Merino-Dìez[1], Roland Hany[3], Harald Brune[2], Oliver Gröning[1], and Roland Widmer[1,*]

[1]*Empa, Swiss Federal Laboratories for Materials Science and Technology, nanotech@surfaces Laboratory, 8600 Dübendorf, Switzerland*
[2]*Institute of Physics, École Polytechnique Fédérale de Lausanne, Laboratory of Nanostructures at Surfaces, CH-1015 Lausanne, Switzerland*
[3]*Empa, Swiss Federal Laboratories for Materials Science and Technology, Laboratory for Functional Polymers, 8600 Dübendorf, Switzerland*

Table of Contents

Deposition of ex-situ synthesized 1,4-triazoles on PdGa:A($\bar{1}\bar{1}\bar{1}$)Pd$_3$

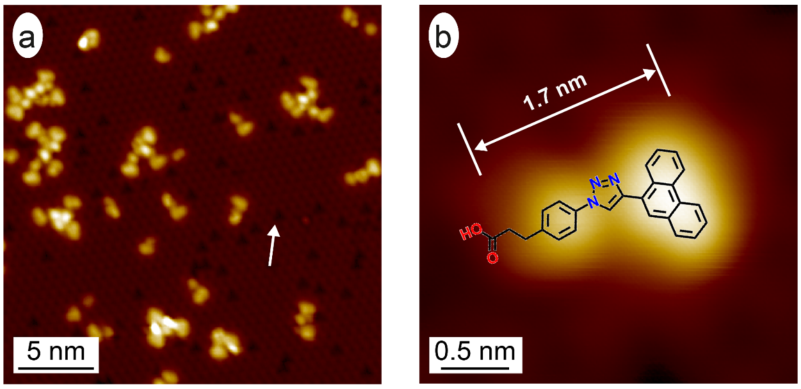

Figure S1

STM images of ex-situ synthesized 1,4-triazoles deposited on the PdGa:A($\overline{111}$)Pd$_3$ surface at 300 K (**a** $V_B = 50\ mV$; $I_T = 20\ pA$; **b** $V_B = 50\ mV$; $I_T = 50\ pA$).

XPS of APA on PdGa:A($\bar{1}\bar{1}\bar{1}$)Pd$_3$, PdGa:A(111)Pd$_1$ and Cu(111)

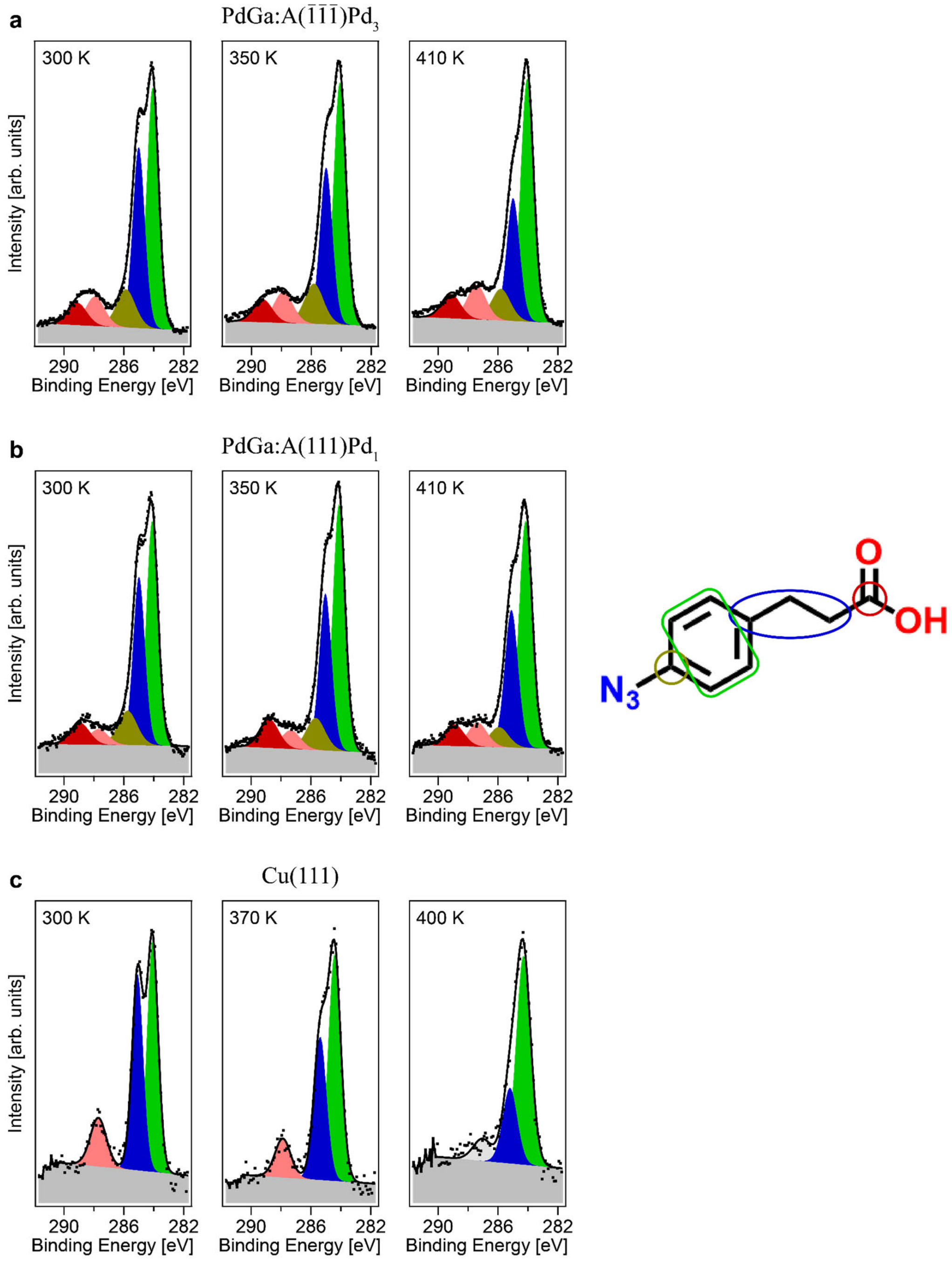

Figure S2

C 1s XPS core level signal of APA on **a** PdGa:A($\bar{1}\bar{1}\bar{1}$)Pd$_3$, **b** PdGa:A(111)Pd$_1$, and **c** Cu(111) after deposition at 300 K (left) and after annealing to the temperatures indicated in the top left corner of each XPS spectrum. On the right a sketch of the APA molecule is displayed with the carbon atoms contributing to each part of the XPS signal is colored according to the colors of the individual components in the XPS spectra. The carboxylic acid contributes two components to the XPS spectra, one corresponding to its inert state (dark red), and the other to the formation of carboxylate (bright red).

PdGa:A($\bar{1}\bar{1}\bar{1}$)Pd_3

	300 K		350 K		410 K	
	BE [eV]	Weighting	BE [eV]	Weighting	BE [eV]	Weighting
COOH	289.2	6.3	289.3	6.6	289.2	7.1
COO-	288	8.3	287.9	8.8	287.5	10.2
C-N	285.8	10.9	285.9	11.4	285.9	9.3
"C3"	285.1	32.8	285.1	28.8	285.1	24.7
"C4"	284.2	43.7	284.2	44.5	284.2	48.8

Table S1

Fitting parameters for the XPS spectra of APA on PdGa:A($\bar{1}\bar{1}\bar{1}$)Pd_3 for the temperatures indicated in Figure S2a. For each temperature, the binding energy (BE) and weight of all fit components depicted in the molecular structure in Figure S2 are given.

PdGa:A(111)Pd_1

	300 K		350 K		410 K	
	BE [eV]	Weighting	BE [eV]	Weighting	BE [eV]	Weighting
COOH	289.0	7.0	288.9	8.5	289.0	6.7
COO-	287.8	5.1	287.4	5.5	287.5	7.5
C-N	285.9	11.0	285.8	9.4	286.0	9.3
"C3"	285.1	33.0	285.1	29.7	285.2	30.0
"C4"	284.2	44.0	284.2	46.8	284.3	49.5

Table S2

Fitting parameters for the XPS spectra of APA on PdGa:A(111)Pd_1 for the temperatures indicated in Figure S2b. For each temperature, the binding energy (BE) and weight of all fit components depicted in the molecular structure in Figure S2 are given.

Cu(111)

	300 K		370 K		400 K	
	BE [eV]	Weighting	BE [eV]	Weighting	BE [eV]	Weighting
COOH	-	0	-	0	-	0
COO-	287.9	14.1	288	11.6	-	0
C-N	-	0	-	0	-	0
Unknown	-	0	-	0	287.2	8.9
"C3"	285.2	39.5	285.5	34.2	285.4	24.2
"C4"	284.2	46.4	284.6	54.1	284.5	66.9

Table S3

Fitting parameters for the XPS spectra of APA on Cu(111) for the temperatures indicated in Figure S2c. For each temperature, the binding energy (BE) and weight of all fit components depicted in the molecular structure in Figure S2 are given.

Supplementary Note 1

For reactivity investigations, we are mainly interested in the two - out of the overall 9 - C atoms of the APA molecule (cf. Figure S2) that are either part of propionic acid, or directly connected to the azide group. Each of these two C atoms in APA give rise to a component in the C 1s core level signal with a chemical shift to higher binding energy with respect to the remaining 7 C atoms of the backbone with an expected weight of 11%.

Because no information is found on the chemical shift in the XPS of the C 1s core level induced by azide functional groups,[1] we identify the contribution of the C atom attached to the azide group to the C 1s XPS signal by referring to Ref. [2], where an XPS investigation of a molecule with a diazo group was performed. The carbon atom attached to the diazo group has been reported to give rise to a C 1s component shifted by about 1 eV towards higher binding energy (but still a lower shift than for carbon in carboxylic groups) with respect to the C 1s component of aromatic carbon atoms. We therefore assign the components denoted with C-N in Table S1-Table S3 to originate from the carbon atom attached to the azide group.

For APA on the PdGa$\{111\}$ surfaces this C-N XPS component is discernible with an amount of 6-11% (depending on the fitting constraints), whereas it is lacking for APA on Cu(111). Based on the N 1s core level XPS signal on Cu(111), we estimate that only 25% of the expected N 1s signal for inert APA is detected, which indicates a large quantity of the azide groups to be detached from APA, in agreement with previous reports on Cu(111).[1]

Contrary to azide functional groups, detailed XPS investigations on carboxylic acids have been reported on Au(111), Ag(100), Ag(111), Cu(100), Cu(110) and Cu(111) surfaces.[3–9] In XPS, this functional group can be identified due to the large chemical shift in the C 1s core level signal towards higher binding energy compared to aromatic carbon, resulting in a C 1s core level component at about 289.3 eV. Upon deprotonation of the COOH group, a new C 1s core level component emerges at around 288.1 eV.[8,9]

Applying these results to our XPS experiments in Figure S2 and Table S1-Table S3above, we find that the carboxylic acid of the APA molecules form a carboxylate upon deposition at 300 K on the Cu(111) surface. Contrary to the PdGa$\{111\}$ surfaces where more than 40% (Pd$_3$-terminated PdGa$\{111\}$) or even close to 60% (Pd$_1$-terminated PdGa$\{111\}$) of all carboxylic acids remain protonated. This ratio remains stable even upon annealing to 350 K. Moreover, while on Cu(111), the XPS signal originating from the carboxylic acid group vanishes upon annealing to 400 K, it persists on PdGa$\{111\}$ up to temperatures of 410 K with a weighting of maximal 17%.

We also determined the experimental C 1s/N 1s XPS intensity ratio for APA and ex-situ synthesized 1,4-triazoles on PdGa:A(111)Pd$_1$ and PdGa:A($\bar{1}\bar{1}\bar{1}$)Pd$_3$ to estimate the upper limit of relative coverage of pristine APA molecules and to determine their thermal stability.

As seen in Table S4 and Table S5, the determined C 1s/N 1s XPS intensity ratio is about a factor of 3 for PdGa:A($\bar{1}\bar{1}\bar{1}$)Pd$_3$ and 3.5 for PdGa:A(111)Pd$_1$ larger than expected - i.e., 7.0 and 7.9 instead of 2.2 - if we assumed all ex-situ synthesized 1,4-triazoles to be pristine. This implies that at most around 30% of all APA molecules exhibit an intact azide group required for the azide-alkyne Huisgen cycloaddition – which is similar to the percentage that has been reported for 4-azidobiphenyl on Cu(111).[1] Nevertheless, the pristine APA molecules co-deposited with 9-EP are thermally stable on PdGa:A(111)Pd$_1$, at least to the reaction temperature because the C 1s/N 1s XPS intensity ratio is roughly the same for APA and 9-EP co-deposited at 300 K and after annealing to the reaction temperature.

To obtain a reasonable core level signal in XPS, we had to prepare samples with high coverage of 9-EP and APA molecules as shown in Figure S4b. Therefore, the amount of reaction products is low due to the reduced mobility of the molecules at such coverage.

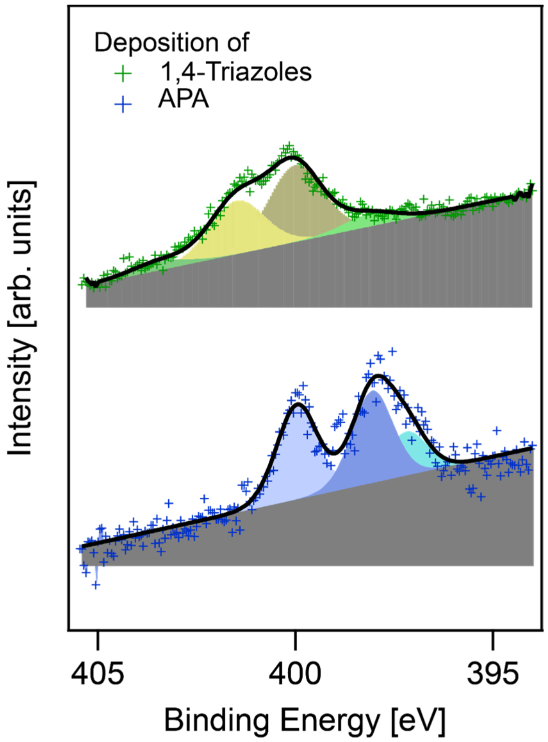

Figure S3

N 1s XPS signal of ex-situ synthesized 1,4-triazoles (upper curve) and APA (lower curve) deposited at 300 K on PdGa:A(111)Pd_3. The markers represent the experimental XPS data, the solid grey areas the background, the colored areas the individual N 1s components and the solid overall fitted intensity.

	APA	1,4-triazoles
C1s/N1s	7.0 (2.2)	6.4

Table S4

Experimental C 1s/N 1s XPS intensity ratios for APA and ex-situ synthesized 1,4-triazoles adsorbed on the PdGa:A($\bar{1}\bar{1}\bar{1}$)Pd_3 surface. The number in brackets for the case of APA molecules corresponds to the expected N 1s/C 1s XPS intensity ratio under the assumption that all 1,4-triazoles remain pristine upon deposition.

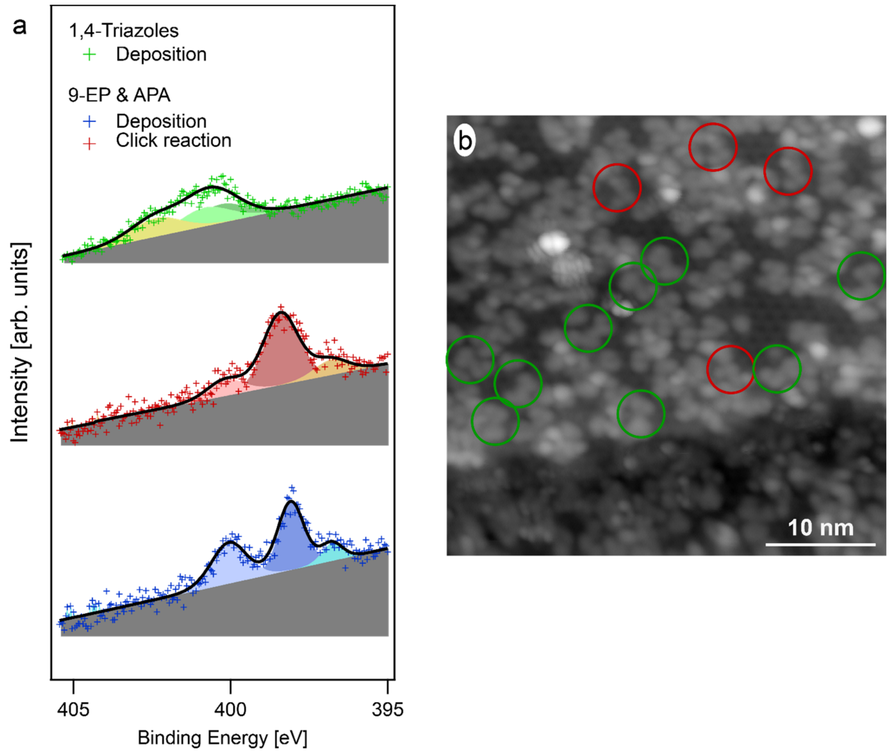

Figure S4

a N 1s signal of ex-situ synthesized 1,4-triazoles deposited at 300 K, APA co-adsorbed with 9-EP at 300 K and after triggering the reaction on PdGa:A(111)Pd$_1$. The markers represent the experimental XPS data, the solid black areas the background, the colored areas the individual N 1s components and the solid overall fitted intensity. **b** STM image ($V_B = -500\ mV; I_T = 10\ pA$) illustrating the coverage of co-deposited 9-EP and APA after initializing the click reaction. Marked in red are the reaction products and in green 9-EP dimers.

	APA	1,4-triazoles	APA & 9-EP	APA & 9-EP (reaction)
C1s/N1s	7.9 (2.2)	6.0	13.9	12.9

Table S5

Experimental C 1s/N 1s XPS intensity ratios for APA, ex-situ synthesized 1,4-triazoles, and APA and 9-EP adsorbed on the PdGa:A(111)Pd$_1$ surface. The number in brackets for the case of APA molecules corresponds to the expected N 1s/C 1s XPS intensity ratio, when assuming all 1,4-triazoles to be pristine.

Temperature evolution of APA on PdGa:B($\bar{1}\bar{1}\bar{1}$)Pd$_1$

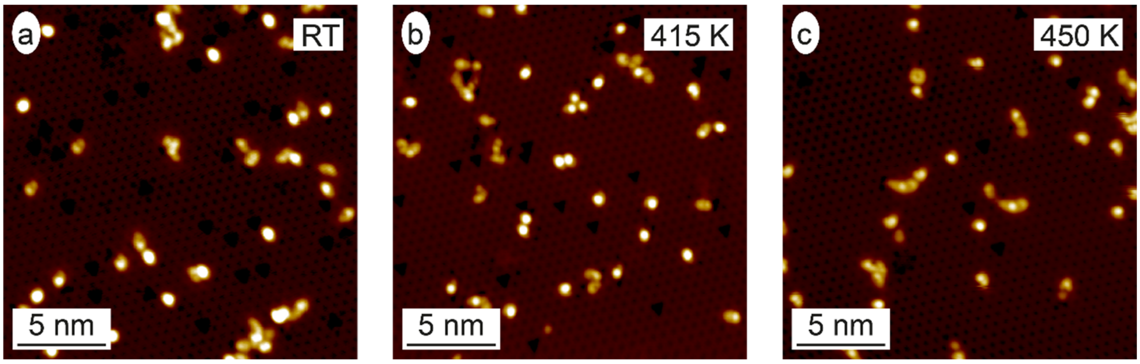

Figure S5
STM images ($V_B = 200\,mV$; $I_T = 200\,pA$) of APA molecules after **a** room temperature deposition, subsequent annealing to **b** 415 K and **c** 450 K.

From room temperature to 415 K, APA appears mostly isolated and in the four configurations shown in Figure 3c-f of the main text. Only upon annealing to 450 K, agglomeration becomes more frequent and the configurations shown in Figure 3c,e of the main text completely disappear.

Ex-situ synthesized 1,4-triazoles deposited on PdGa:A(111)Pd$_1$

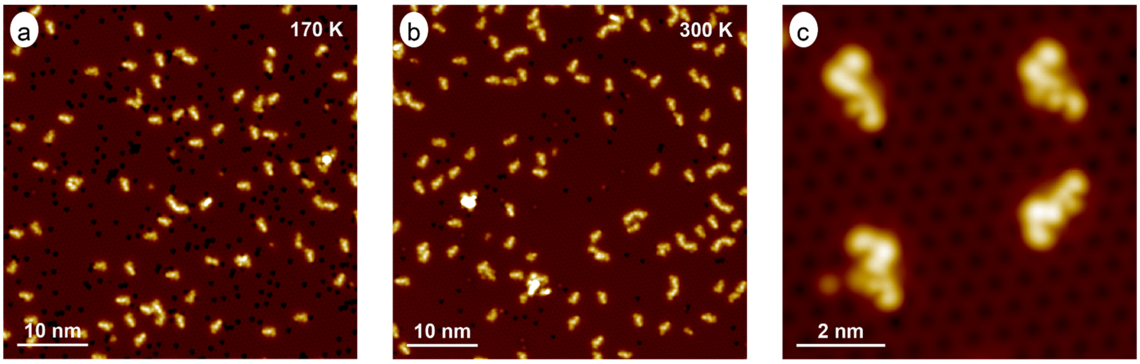

Figure S6

STM images ($V_B = 1000\ mV; I_T = 20\ pA$) of the ex-situ synthesized 1,4-triazoles deposited at **a** 170 K and **b** 300 K. In **c**, the STM signatures ($V_B = 50\ mV; I_T = 100\ pA$) of the three observed adsorption configurations of deposited 1,4-triazoles are depicted.

Sample	ex-situ synthesized 1,4-triazoles		
	S_{P1*} 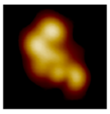	S_{P2*} 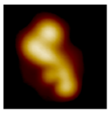	R_{P2*} 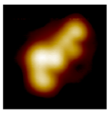
A:Pd$_1$	9 ± 2%	39 ± 3%	52 ± 4%

Table S6

Relative abundance of the adsorption configurations of ex-situ synthesized 1,4-triazoles on PdGa:A(111)Pd$_1$ at 300 K.

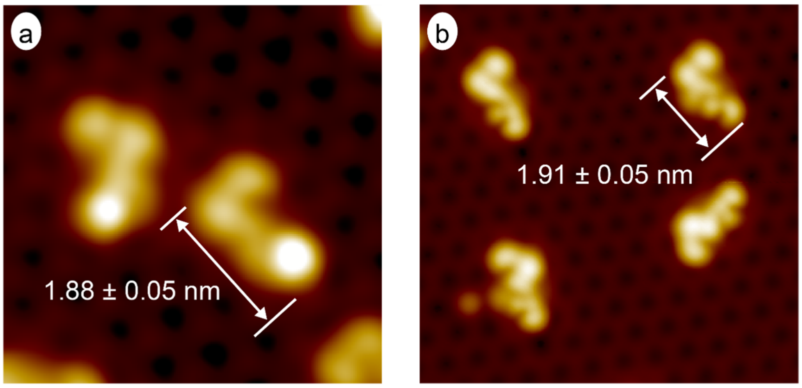

Figure S7

STM images of **a** the on-surface synthesized reaction products between 9-EP and APA and **b** ex-situ synthesized 1,4-triazoles on Pd$_1$-terminated PdGa{111} surfaces.

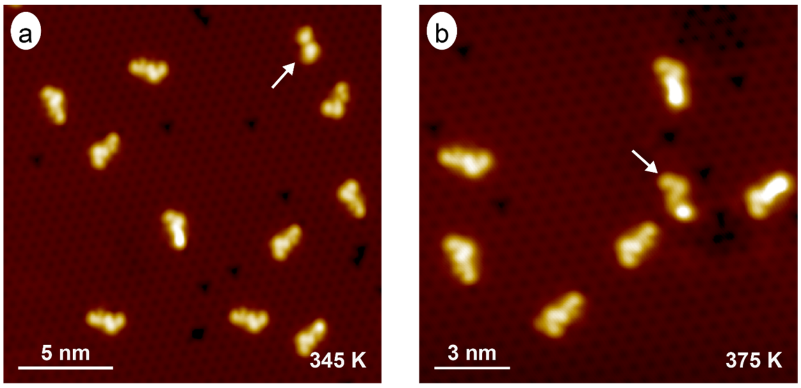

Figure S8
STM images of the ex-situ synthesized 1,4-triazoles after annealing to **a** 345 K ($V_B = 50\ mV$; $I_T = 100\ pA$) and **b** 375 K ($V_B = 50\ mV$; $I_T = 20\ pA$). The white arrows indicate molecular structures that are identical to the ones obtained by on-surface synthesis between APA and 9-EP on the Pd_1-terminated PdGa$\{111\}$ surfaces.

Abundance of reaction products

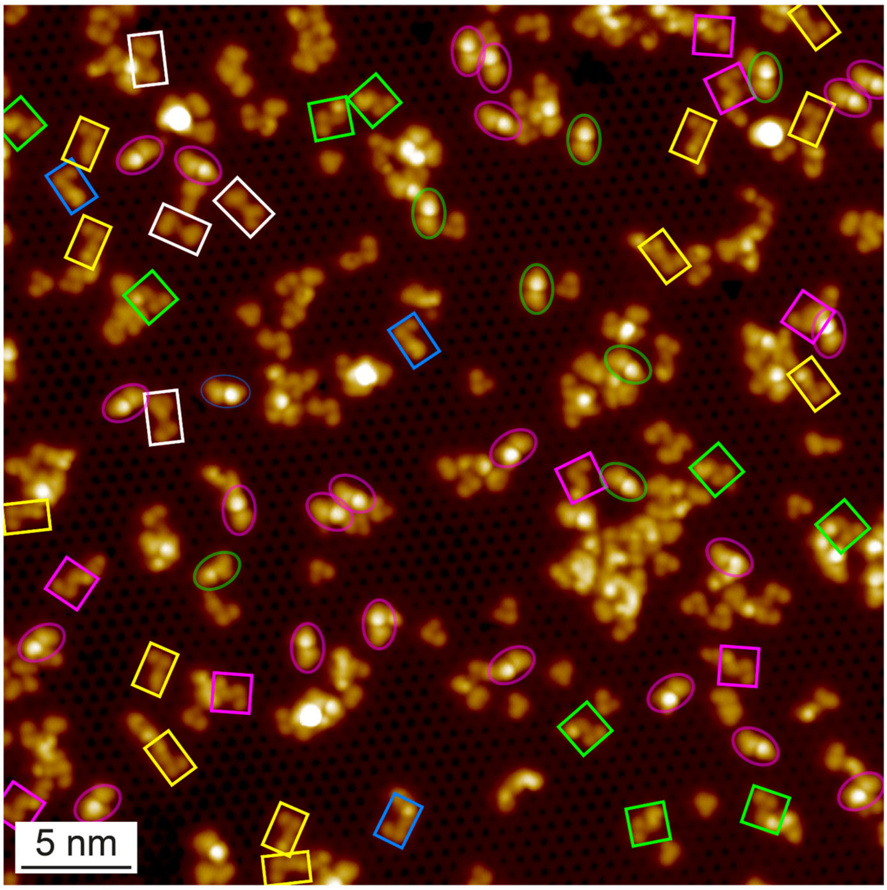

Figure S9

40 x 40 nm^2 STM image after thermally triggering the azide-alkyne Huisgen cycloaddition on the PdGa:B($\bar{1}\bar{1}\bar{1}$)Pd$_1$ ($V_B = 100\ mV$; $I_T = 100\ pA$) by annealing to 425 K. All 1,4-triazoles and 9-EP dimers are highlighted by colored rectangles or circle (see text).

Supplementary Note 2

The colors of the rectangles and circles in Figure S9 and Figure S10 indicate the same reaction product. Yellow rectangles correspond to R$_{P1}$, the blue ones to S$_{P1}$, the green ones to R$_{P2}$, the pink ones to S$_{P2}$ and the white ones to 9-EP dimers. The red circles highlight the S$_{P3}$ and the green circles the R$_{P3}$ 1,4-triazole, respectively. For the statistical analysis, no structures belonging to larger molecule agglomerations are considered, as can be seen from Figure S9 and Figure S10. As a consequence, the determined yield of reaction products given in Table S7 potentially underestimates the actual yield.

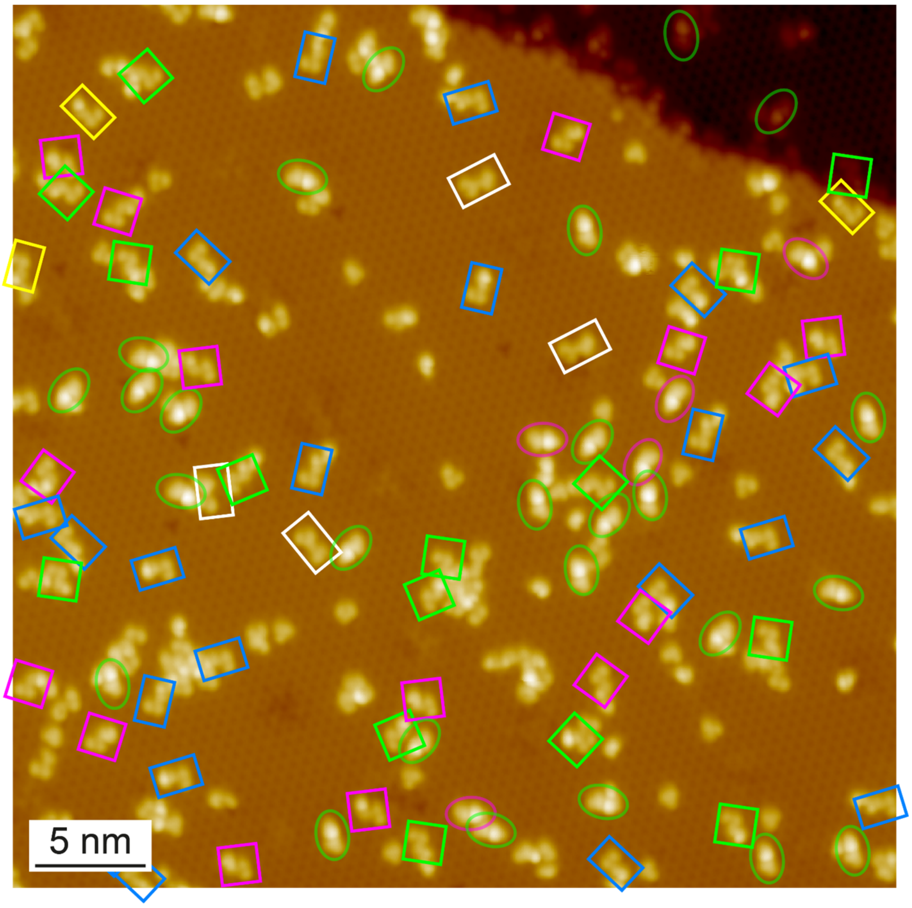

Figure S10
40 x 40 nm^2 STM image after thermally triggering the azide-alkyne Huisgen cycloaddition on the PdGa:A(111)Pd$_1$ ($V_B = 100\ mV$; $I_T = 100\ pA$) by annealing to 425 K. All 1,4-triazoles and 9-EP dimers are highlighted by colored rectangles or circles (see text).

Side products of the azide-alkyne Huisgen cycloaddition on Pd$_1$-terminated PdGa{111} surfaces

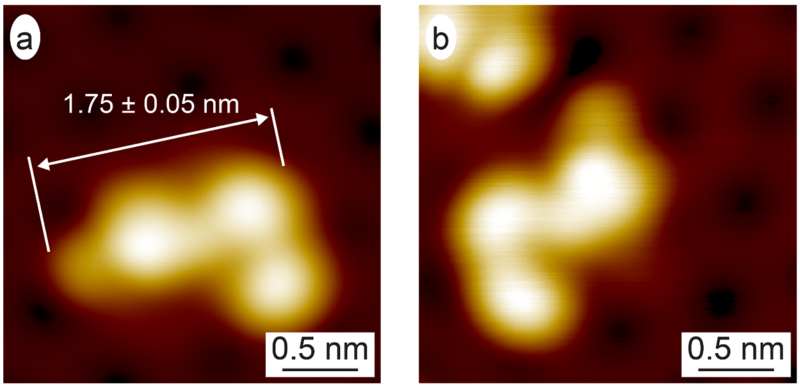

Figure S11
STM images (**a** V_B = 50 mV, I_T = 250 pA; **b** V_B = 10 mV, I_T = 5 pA) of side products of the azide-alkyne Huisgen cycloaddition on Pd$_1$-terminated PdGa{111} surfaces. These side products are probably 9-EP coupled to the phenylpropionic acid originating from azide decomposition of APA molecules.

DFT simulations of 1,4- and 1,5-triazoles

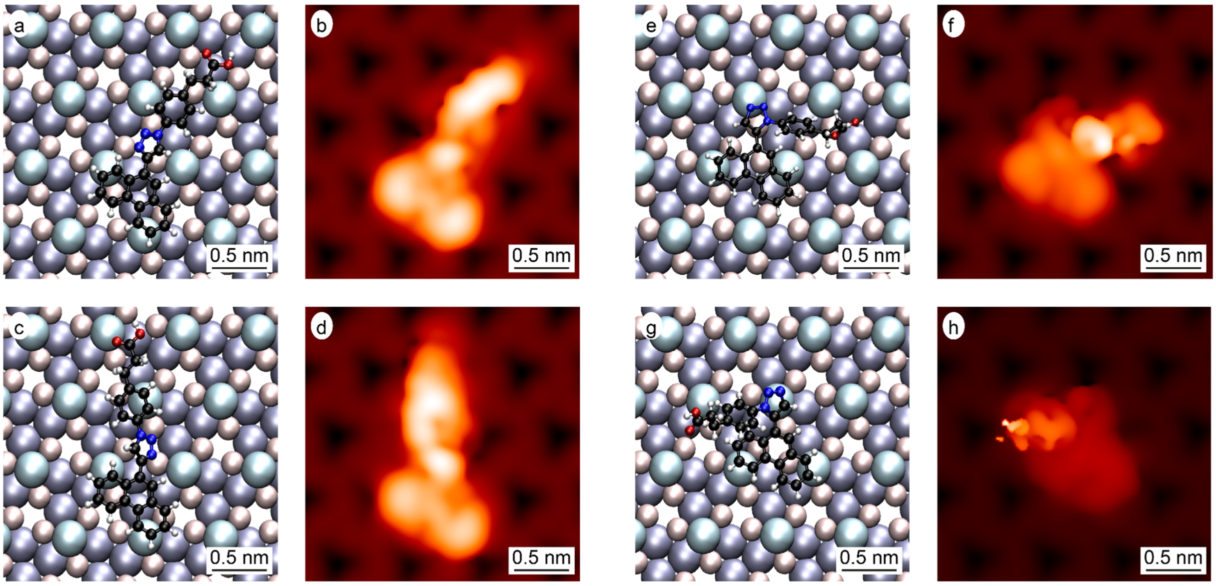

Figure S12

DFT-optimized adsorption configurations (**a,c,e,g**) with the corresponding DFT-simulated STM signature (**b,d,f,h**) for **a-d** 1,4-triazoles and **e-h** 1,5-triazole diastereomers. The two diastereomers of the 1,4- and 1,5-triazoles exhibit the same adsorption configuration in their phenanthrene unit, while the remaining atoms are rotated by 180° around the bond connecting the phenanthrene with the triazole unit.

Adsorption configurations of the 1,4-triazoles

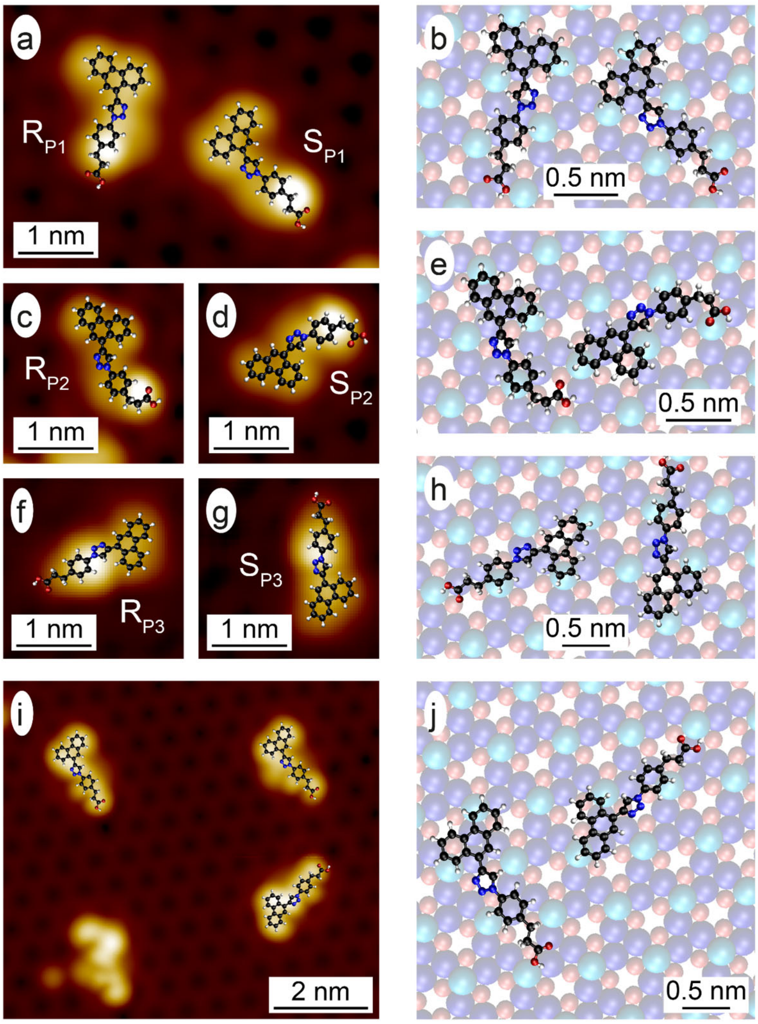

Figure S13
STM images of the 1,4-triazoles by on-surface synthesis between APA and 9-EP on the PdGa:B($\bar{1}\bar{1}\bar{1}$)Pd$_1$ surface overlaid with the molecular structures in **a**, **c-d**, **f-g** and the corresponding adsorption configurations in **b**, **e**, **h. i** STM images of the ex-situ synthesized 1,4-triazoles and **j** the corresponding adsorption geometries.
The adsorption geometries of the ex-situ synthesized 1,4-triazoles in **j** correspond to the ones shown in **b** and **e**.

Determination of reaction yield

Substrate	#APA / 100 nm^2	#9-EP / 100 nm^2	#1,4-triazole / 100 nm^2	Yield
A:Pd$_1$	6.07	8.04	2.24	37%
B:Pd$_1$	8.75	6.10	3.57	58%

Table S7

The number of APA and 9-EP molecules per 100 nm^2 after RT deposition on the A:Pd$_1$ and B:Pd$_1$ surfaces, respectively. The number of 1,4-triazoles per 100 nm^2 after subsequent annealing to 425 K. The reaction yield is determined by the formula: $Yield = 100\% * \frac{actual\ yield}{yield} = 100\% * \frac{\min(APA/100nm^2, 9-EP/100nm^2)}{1,4-triazole/100nm^2}$.

Supplementary References

1. Bebensee, F. *et al.* On-Surface Azide–Alkyne Cycloaddition on Cu(111): Does It “Click” in Ultrahigh Vacuum? *J. Am. Chem. Soc.* **135**, 2136–2139 (2013).
2. Liu, L. *et al.* α-Diazo Ketones in On-Surface Chemistry. *J Am Chem Soc* **140**, 6000–6005 (2018).
3. Gao, H.-Y. *et al.* Decarboxylative Polymerization of 2,6-Naphthalenedicarboxylic Acid at Surfaces. *J Am Chem Soc* **136**, 9658–9663 (2014).
4. Wasio, N. A. *et al.* Self-assembly of hydrogen-bonded two-dimensional quasicrystals. *Nature* **507**, 86–89 (2014).
5. Franke, M. *et al.* Temperature-dependent reaction of phthalic acid on Ag(100). *J. Phys. Chem. C* **119**, 23580–23585 (2015).
6. Morchutt, C. *et al.* Interplay of Chemical and Electronic Structure on the Single-Molecule Level in 2D Polymerization. *ACS Nano* **10**, 11511–11518 (2016).
7. Lipton-Duffin, J., Abyazisani, M. & MacLeod, J. Periodic and nonperiodic chiral self-assembled networks from 1,3,5-benzenetricarboxylic acid on Ag(111). *Chem. Commun.* **54**, 8316–8319 (2018).
8. Abyazisani, M., Bradford, J., Motta, N., Lipton-Duffin, J. & MacLeod, J. Adsorption and Reactivity of Pyridine Dicarboxylic Acid on Cu(111). *J Phys Chem C* **122**, 17836–17845 (2018).
9. Abyazisani, M., Bradford, J., Motta, N., Lipton-Duffin, J. & MacLeod, J. Adsorption, Deprotonation , and Decarboxylation of Isophthalic Acid on Cu(111). *Langmuir* **35**, 7112–7120 (2019).